Applied Materials Today 40 (2024) 102408

Contents lists available at ScienceDirect

Applied Materials Today

journal homepage: www.elsevier.com/locate/apmt

Improving the synthesis of heterogeneous catalysts by gliding arc plasma using the "no-cooling system"

Fanny Hanon, Eric Michel Gaigneaux *

Institute of Condensed Matter and Nanosciences (IMCN), Université catholique de Louvain (UCLouvain), Place Louis Pasteur 1, Louvain-la-Neuve 1348, Belgium

ARTICLE INFO

Keywords:
Glidarc plasma
Post-discharge
Catalysts
(Hydr)oxides
Maturation
No-cooling

ABSTRACT

Glidarc plasma (GP) is a promising method for preparing heterogeneous catalysts due to its mild conditions and short processing time. This technique has been used to synthesize various catalysts like FeOx and MnOx. Adding a post-discharge (PD) step during synthesis has been shown to impart valuable new properties, such as phase transformation, increased specific surface area, and enhanced catalytic activity. Knowing that the PD step mostly impacts the plasma-synthesized solids maturation and can be accelerated if heat is introduced into the system, we now contemplate the possibility of accelerating the GP catalysts synthesis by allowing the solution to be heated by the energy spontaneously provided by the plasma without the necessity to add a PD. To challenge this approach, we subjected $FeSO_4$ and $SnSO_4$ precursors to plasma exposure without employing the cooling system usually integrated in the GP set-up and compared the resulting solids with those obtained via conventional GP synthesis involving a PD step. The findings show that for iron precursors, the absence of cooling accelerates the formation of non-catalytically active phases and causes particle agglomeration, which is undesirable. However, for tin precursors, the absence of a cooling system introduces features that further improve the catalytic activity of the solids. Precisely, tin oxide phases developed better than other less-catalytically active ones without affecting the textural properties of the solid. This suggests that in some cases, eliminating the PD step can simplify the GP catalyst synthesis process and reduce its environmental and economic impact.

1. Introduction

Glidarc plasma (GP) synthesis appears to be an interesting alternative approach for the preparation of heterogeneous catalysts. As a matter of fact, nowadays, the goal to reduce the environmental and economic impact of industrial processes is primordial, and a widely employed strategy to achieve this objective is the utilization of a catalyst [1–3]. Consequently, developing innovative methods facilitating the synthesis of catalysts with interesting characteristics such as selectivity, activity, stability, mechanical and thermal resistances, and recyclability in a greener, quicker, and less expensive manner, is a field of substantial interest [1,4–6]. In this context, the GP emerges as an interesting alternative when compared to other synthesis methods due to its requirement only for mild conditions and its short processing time. Moreover, this approach is deemed to be eco-friendly and cost-effective, as the sole chemical agent employed to generate reactive species is water-saturated air [7].

The glidarc plasma reactor was conceived by H. Lesueur and later refined by A. Czernichowski in 1988. It consists of two stainless steel electrodes with a divergent profile connected to a high voltage generator (Fig. 1) [8,9]. An arc is formed at the smallest distance between the electrodes when the generator is activated. This arc glides along the electrodes thanks to a flow of gas (named plasma gas) that is sent perpendicular to them. At the end of the electrodes, where the distance is too big to maintain the arc, it breaks and a new arc forms (Fig. 1). In this system, the arc constitutes the thermal part of the plasma. The gliding process allows the formation of what is called the "plume", characterized by the cooling of the arc to nearly ambient temperature, resulting in the formation of the quenched plasma at atmospheric pressure. Consequently, due to its composition of both thermal and non-thermal plasmas, the GP is classified as a "temperate" plasma [8, 10–15].

The interaction between the arc and the plasma gas creates the "primary species", which can subsequently undergo reactions among themselves or with parent species, leading to the formation of "secondary species" (Fig. 1). This system is capable of generating various types of reactive species, however, when humid air is employed as the plasma gas, the predominant species formed are primarily acidic and

* Corresponding author.
E-mail address: eric.gaigneaux@uclouvain.be (E.M. Gaigneaux).

https://doi.org/10.1016/j.apmt.2024.102408
Received 2 May 2024; Received in revised form 14 August 2024; Accepted 22 August 2024
Available online 28 August 2024

oxidative. These characteristics have resulted in the utilization of GP in diverse applications, including gas depollution or valorisation, wastewater treatment, surface modification of solid materials, and the synthesis of heterogeneous catalysts [7,15–20]. The interaction of a metal precursor solution with the plasma-generated species from the plume enables the formation of a precipitate that can be used as a catalyst. Several types of catalysts have already been synthesized through this method, including metal (hydr)oxides (TiO_2, FeO_x, MnO_2, SnO_2) and supported catalysts (FeO_x/Kaolinite, TiO_2/SnO_2). These catalysts exhibit interesting properties and catalytic activity when used for pollutant degradation in both gas and liquid phases [7,16,17,21–24].

It has also been observed that including a post-discharge (PD) step in GP synthesis can impart valuable new properties, such as phase transformation, increased specific surface area, and enhanced catalytic activity (Fig. 1, Table 1) [7,25]. The PD step consists of exposing the precursor solution to GP, turning off the discharge, and allowing the suspension to stand outside the reactor for a defined duration at a fixed temperature. While this procedure is intriguing for the development of more valuable catalysts, it comes with the drawback of prolonging the synthesis duration and potentially requiring additional energy input into the system.

The PD step actually mostly consists of transforming the plasma-synthesized solid by allowing its maturation. Furthermore, accelerating this growing process often goes with introducing heating to the system during this step [26]. Therefore, to further optimize the approach, we contemplated the possibility of accelerating the maturation of GP-synthesized solids by applying heat directly during the plasma exposure. In conventional plasma synthesis, the GP reactor and the exposed solution are cooled down using a double jacket with circulating cold water. Consequently, we explored the idea of omitting this cooling system, i.e. allowing the solution to get heated by the energy spontaneously provided by the plasma, and checked whether this is enough to induce rapid maturation.

To challenge this hypothesis, we exposed various types of iron and tin precursors to the plasma without using the cooling system and compared the resulting solids with those obtained from conventional GP synthesis, where the cooling system was employed during the exposure, and which involved a PD step at 100 °C or 25 °C afterward. If successful, the "no-cooling system" would considerably reduce both the synthesis time and energy provided to the system, while still producing solids with characteristics closely resembling those obtained by incorporating a PD step. This would align with the broader objective of developing interesting catalysts through this innovative, economically viable, and environmentally friendly GP approach. Our focus here is on the synthesis of catalysts dedicated for air depollution by total oxidation of pollutants.

Table 1
Effect of the post-discharge step at 100 °C and 25 °C on solids synthesized from iron precursors ($(NH_4)_2Fe(SO_4)_2$ and $FeSO_4$) and tin precursors ($SnSO_4$ and $SnCl_2$) [26].

	Iron precursors ($(NH_4)_2Fe(SO_4)_2$ and $FeSO_4$)		Tin precursors ($SnSO_4$ and $SnCl_2$)	
	PD at 100 °C for 3 h	PD at 25 °C for 72 h	PD at 100 °C for 3 h	PD at 25 °C for 72 h
Mass of solid produced	↗*	↗↗	= for $SnSO_4$; ↗↗ for $SnCl_2$	= for $SnSO_4$; ↗ for $SnCl_2$
Phases developed	↗↗ of Fe_2O_3, ↗↗ of $Fe_2(SO_4)_3$, ↘↘ of $FeOHSO_4$	↗ of Fe_2O_3, ↗of $Fe_2(SO_4)_3$, ↘ of $FeOHSO_4$	SnO_2	
% of S or Cl presents in the solid	↘**	↘	↘	↘↘
Specific surface area	↗↗	↗	↘	↘↘
Pore volume	↗↗	↗	=	
Catalytic activity	↗↗	↗ for $(NH_4)_2Fe(SO_4)_2$; ↘ for $FeSO_4$	↗	↗↗

*↗: increase; **↘: decrease.

Since this approach has never been used before, our research, and accordingly this contribution, has been structured as follows. (i) First, we have determined how intense was the heating naturally occurring from the plasma discharge, and whether it could cause the exposed solution to evaporate too quickly, thereby altering the conditions during exposure. (ii) Then the impact of using (or not) the cooling system during the plasma exposure of the metals precursors solutions is investigated via the characterization of the surface (probed by XPS), the bulk (probed by DRX, EDX, SEM) and the catalytic performance of respectively recovered solids. (iii) Finally, as the no-cooling approach has not been tested before in GP-catalysts synthesis, we have sought at investigating the difference between letting heat the precursor solution during exposure along the no cooling approach, *vs* using the cooling system during exposure but heating the precipitating solids after the GP, applying the post-discharge approach. Among others, this consisted in comparing the characteristics of our different solids with those obtained

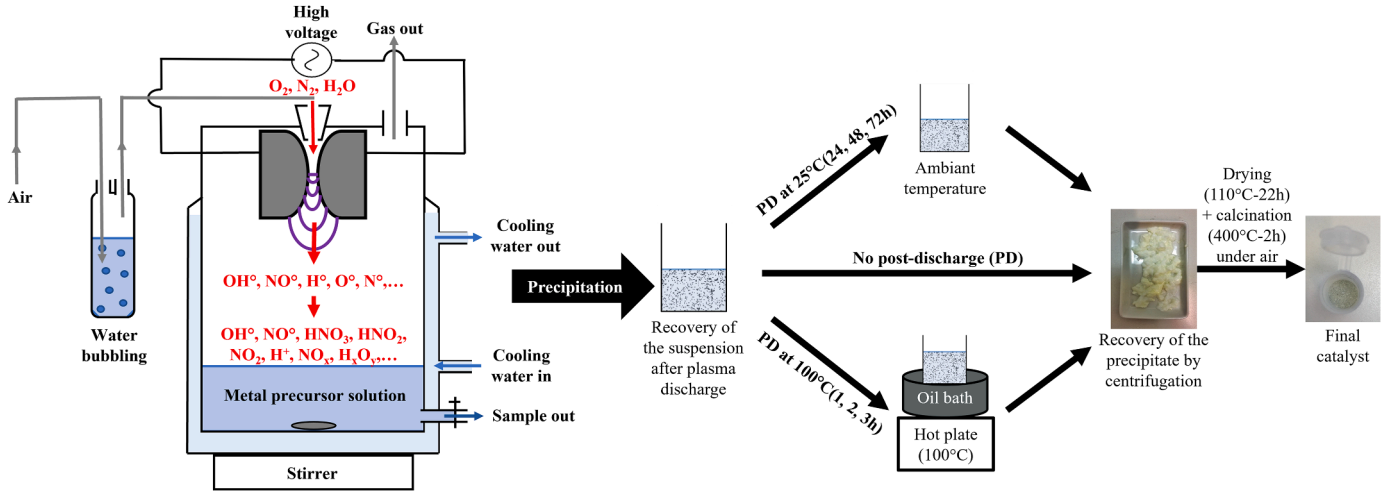

Fig. 1. Scheme of glidarc plasma reactor, species mainly present in a humid air glidarc plasma [15] and scheme of catalysts synthesis with and without a post-discharge step.

from other methods in the literature.

2. Materials and methods

2.1. Materials

Iron(II) sulfate heptahydrate ($FeSO_4.7H_2O$; ≥ 99%), tin(II) sulfate ($SnSO_4$; ≥ 95%) and tin(II) chloride ($SnCl_2$; ≥ 99%) were purchased from Sigma Aldrich and ammonium-iron(II) sulfate hexahydrate ($(NH_4)_2Fe(SO_4)_2.6H_2O$; ≥ 99%) from Roth.

2.2. Methods

2.2.1. Synthesis device: the GP reactor

The gliding arc plasma setup employed in this study comprises the following components (Fig. 1):

- A high voltage generator (ABL Transformer; 9kV; 100mA) connected to both stainless-steel electrodes with a divergent profile, positioned within the reactor.
- A gas supply setup consisting of a compressed air source, a saturator filled with water in which air is bubbled and a mass flow controller controlling the gas flow rate (fixed at ≈ 400L/h).
- A central reactor in the form of a double-walled cylindrical glass tube. It features inlets and outlets for the circulation of an external cooling fluid (water from the tap), an additional inlet for the nozzle to direct the air flow between the electrodes, and an opening for gas exhaust (to prevent exceeding pressure within the reactor). An outlet valve is also present to facilitate retrieval of the reactor content following plasma exposure.

2.2.2. Materials synthesis

In the initial step, demineralized water was exposed to the GP without employing the cooling system for 1 h, and the temperature of the solution was monitored every 5 min. This was done to investigate the influence of not utilizing the cooling system on the heating of the solution.

The precursor solutions were prepared by dissolving these compounds in deionized water. Subsequently, 450 mL of the respective solutions were introduced into the reactor, stirred magnetically (1 rotation/s) and exposed to the plasma discharge for 45 min for $(NH_4)_2Fe(SO_4)_2.6H_2O$, 60 min for $FeSO_4.7H_2O$ and 120 min for $SnSO_4.7H_2O$ and $SnCl_2$. Based on previous studies, either from literature or in the lab, these exposure times were chosen to synthesize the catalysts with the best catalytic activity and/or the highest yield of recovered precipitate [23,27]. The optimal exposure time varies depending on the type of precursor used.

To assess the influence of the cooling system, solids were synthesized by either cooling the solution with tap water circulating in the double-jacket during the exposure (samples named " with cooling") or not using the cooling system and allowing the solution to heat up during the exposure (samples named "no cooling"). The solid formed was subsequently recovered by centrifugation (24490G, 30 min) and subjected to two washing cycles with distilled water. All the solids obtained after centrifugation were dried in an oven under air at 110 °C for 22 h ± 2 h and then calcined in a muffle furnace under air at 400 °C for 2 h.

The samples are referenced as follows: "Name of the precursor – no cooling / with cooling".

The resulting solids were compared with those obtained from classical synthesis involving a PD step at 100 °C for 3 h or at 25 °C for 72 h, where the cooling system was employed during the exposure (see complete synthesis protocol in [26]).

2.3. Characterization of the solids formed

All the characterizations presented here were done after calcination of the solids formed, except for the XRD that was done before and after the calcination step.

2.3.1. X-ray diffraction (XRD)

The catalyst, previously ground, is placed on a polished Si single crystal sample holder covered with a thin layer of Nivea© cream and is introduced into a Bruker-D8 Advance diffractometer with a Bragg-Brentano geometry. The X-rays sent to the sample are produced using a copper anode (Kα=0.15418 nm). The analysis is performed for 2θ angles from 5° to 80° with an increment of 0.015° and 0.15s integration time. Detection is performed using a LynxEye XE-T Technology detector. The diffractograms are then processed using the ICDD-PDF2-2004 database [28].

2.3.2. X-ray photoelectron spectroscopy (XPS)

The samples, previously crushed, are placed on a double-sided sticker which is itself placed on a 4 mm diameter stainless steel sample holder placed in an aluminium carousel. The samples are then degassed under ultra-high vacuum at 10^{-5} Pa for 12 h in order to eliminate the physisorbed compounds before being analysed. The machine used is an SSX 100/206 Photoelectrons Spectrometer from Surface Science Instruments (USA). It is equipped with a micro-focused monochromatic Al X-ray source powered at 20 mA and 10 kV. The pressure inside the analysis chamber is 10^{-8} Pa, the analysis angle is 55°. An electron gun operating at 8 eV and a Ni grid placed 3 mm above the sample surface are used to ensure that the sample charge is stabilised during analysis. The data are processed using the CasaXPS program from Casa Software Ltd, UK. To calibrate the binding energy, the C-(C,H) component of the C 1 s peak is positioned at 284.8 eV. The spectra can then be decomposed, and the atomic percentages are obtained using the normalized peak areas, the sensitivity factors provided by the manufacturer and a Shirley-type baseline. The atomic percentages of each element are recalculated by removing the carbon contamination due to the experimentation. From the percentage obtained for O 1 s, the quantity of O atoms bound to the carbonaceous contamination is deduced, considering 3 types of carbon-oxygen bonds: O-C=O; O-C-O and C=O; C-O. The remaining percentages of the elements not coming from the contamination are then brought back to 100%.

2.3.3. Scanning electron microscopy (SEM) and energy dispersive X-ray (EDX)

The ground solids are placed on an adhesive carbon film which is itself deposited on an aluminium support. The scanning electron microscope used is a JEOL 7600F operating between 2 kV for the SEM images (in Gentle Beam High resolution mode (GBH)) and at 15kV for the EDX analyses. The atomic percentages of each element are recalculated by removing carbon, aluminium, chromium and gold contamination. All remaining percentages are then brought back to 100%.

2.3.4. N_2-physisorption

N_2-physisorption is used to measure the specific surface area by the BET method (Brunauer, Emmet and Teller) and the pore volume by the BJH method (Barret-Joyner-Halenda). In practice, the weighed ground solids are introduced into glass tubes with a filler rod in order to limit the error made on the measurement due to the dead volume of the glass tubes. A vacuum degassing of at least 6 h at 140 °C is carried out at a vacuum of approximately 10 mbar. After degassing, the powder is weighed again. Then the glass tube is introduced into a specific surface and porosity analyser (TriStar from Micromeritics). The analysis is carried out using nitrogen at -196 °C in the range of relative pressures from 0.01 to 0.99.

2.3.5. Catalytic test

The catalytic activity of the synthesized solids is evaluated by following their ability to totally oxidize benzene in gas phase at different temperatures (Eq. (1)). The purpose of this test is primarily to

characterize the impact of the modifications introduced to the synthesized solids when the cooling system is not used.

$$C_6H_6 + \frac{15}{2}O_2 \rightarrow 6CO_2 + 3H_2O \quad (1)$$

The catalysts tested are sieved to achieve a particle size ranging between 200 and 315µm. A constant mass of 100 mg of catalyst, mixed with 400 mg of glass beads measuring between 350 and 500µm, is introduced into the reactor between 2 layers of quartz wool so that the catalyst occupies a uniform volume within the reactor. The reaction gas, containing 200 ppm by volume of benzene and 10 vol% O_2, is continuously supplied to the reactor at a flow of 100 mL/min throughout the analysis, with He serving as the carrier gas. The reagent-to-catalyst volume ratio per hour (VVH) is maintained at approximately 60000h^{-1}. The reactor operates within a temperature range from 50 to 400 °C, with increments of 50 °C per stage. At the outlet of the reactor, the gas effluent is directed to a Varian CP-3800 gas chromatograph equipped with a CP-sil 8CB column and a flame ionisation detector (FID). He is used as the GC carrier gas and the analysis is conducted at a constant temperature of 80 °C. To calculate the remaining (not converted) benzene, 4 injections of the reactor outlet gas are performed for each tested temperature.

Calibration is performed based on the benzene peak. It is assumed that at the initial reactor temperature, i.e. 50°C, benzene does not undergo any conversion, and the peak area at this temperature signifies 0% conversion. Using this reference area, the benzene conversion for each temperature stage is calculated using an equation of the following form:

$$\frac{peak\ area\ at\ 50°C - peak\ area\ at\ a\ given\ temperature}{peak\ area\ at\ 50°C} * 100 \quad (2)$$

3. Results and discussion

3.1. Impact of the no cooling system on the temperature of the exposed solution

When demineralized water is exposed to the GP without using the cooling system, the temperature of the solution gradually rises and stabilizes around 60 °C after 1 h of exposure (Fig. 2). This indicates that, although the solution warms up during the exposure, it does not go above the boiling point of water. Consequently, it remains feasible to expose metal solution precursors without significantly changing the volume of the exposed solution, thereby maintaining a consistent distance between the electrodes and the liquid surface.

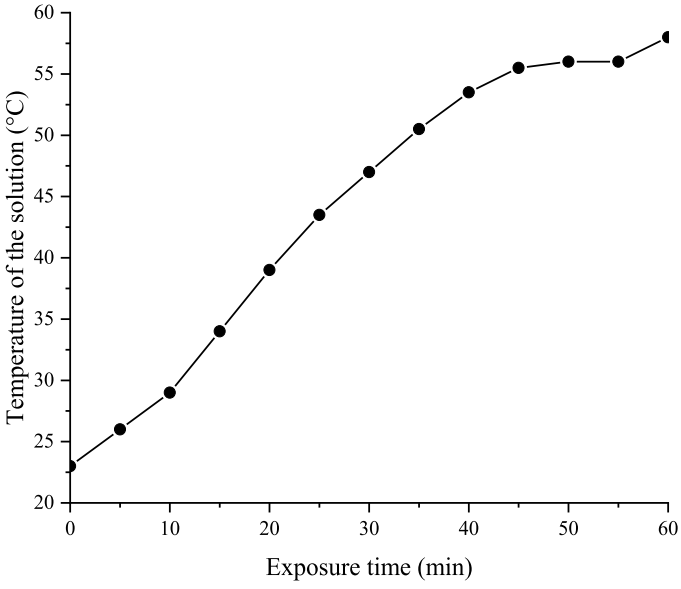

Fig. 2. Temperature of demineralized water exposed to the GP without using the cooling system.

3.2. Impact of the no cooling system on solids GP-synthesized

3.2.1. Iron precursors

Regarding the mass of solids formed from iron precursors, it remains relatively constant with or without the cooling system (Table 2). For the $(NH_4)_2Fe(SO_4)_2$ precursor, the small difference observed between the samples with and without cooling is considered insignificant as the recovered mass is already small, and that some solid is unavoidably lost during the washing steps. The fact that the yield of recovered solids does not increase when the no cooling system is used is likely due to the fact that the exposure time remains identical in both systems, with or without the cooling system. Consequently, the reactive species (HNO_2/NO_2^- [29]) do not have additional time to react with the precursor, as is the case when a PD step is introduced [26].

XRD reveals that for both iron precursors, with or without the cooling system, the resulting solid contains a mixture of hematite (Fe_2O_3) and $FeOHSO_4$. However, the mikasaite ($Fe_2(SO_4)_3$) phase tends to emerge when the cooling system is not utilized, especially in the solid formed from the $(NH_4)_2Fe(SO_4)_2$ precursor (Fig. 3). The appearance of mikasaite can be attributed to the tendency of $FeOHSO_4$ to decompose, particularly under heat, into FeOOH (which transforms into Fe_2O_3 upon calcination) and $Fe_2(SO_4)_3$ (Eq. (3)) [30].

$$3FeOHSO_4 \rightarrow Fe_2(SO_4)_3 + FeOOH + H_2O \quad (3)$$

For the $(NH_4)_2Fe(SO_4)_2$ precursor, XPS reveals the presence of nitrogen as NH_4^+ ions (as indicated by the position of N1s peak around 402 eV), suggesting the likely formation of another phase that was not observed by XRD (Table 3, Appendice A). From the at % of N, we understand that this phase is less present when the cooling system is not used. Moreover, similarly with observations made in classical GP synthesis where the cooling system is used and when a PD step is added, the at % of each element at the surface and in bulk also differs without the cooling system. Therefore, it can be deduced that the absence or presence of the cooling system does not improve the development of a more or less homogeneous (bulk *vs* surface) solid.

Additionally, the binding energy around 169 eV of the S2p peak acquired through XPS confirms the presence of iron sulfate phases in each solid (Table 3, Appendice A). However, although the at % of S measured by XPS is higher than when measured by EDX, suggesting that iron sulfate phases predominantly reside on the outer layer of the solids, the difference between the S at % at the surface and in bulk is less pronounced than in other GP synthesis method. The higher at % of S obtained by EDX for the no-cooling samples indicates that the development of a sulfate phase in bulk is higher in the absence of the cooling system, corroborating findings from XRD analysis (Table 3). These observations can be elucidated through the hypothetical mechanism of formation proposed in [26]. Upon exposure to the GP, iron precursors undergo oxidation, where Fe^{2+} ions are transformed into Fe^{3+} ions by plasma species (Eq. 4). Subsequently, these Fe^{3+} ions can interact either with water to form FeOOH or with SO_4^{2-} from the precursor to form $FeOHSO_4$ (Eqs. (5), (6)). Typically, in systems with the cooling system, there is a higher probability for Fe^{3+} to engage with H_2O molecules due to their higher concentration compared to SO_4^{2-}. However, in systems

Table 2
Mass of solid produced with iron precursors by glidarc plasma with and without cooling system.

	Mass of solid produced (g)
$(NH_4)_2Fe(SO_4)_2$ with cooling	0.050
$(NH_4)_2Fe(SO_4)_2$ no cooling	0.040
$FeSO_4$ with cooling	0.131
$FeSO_4$ no cooling	0.136

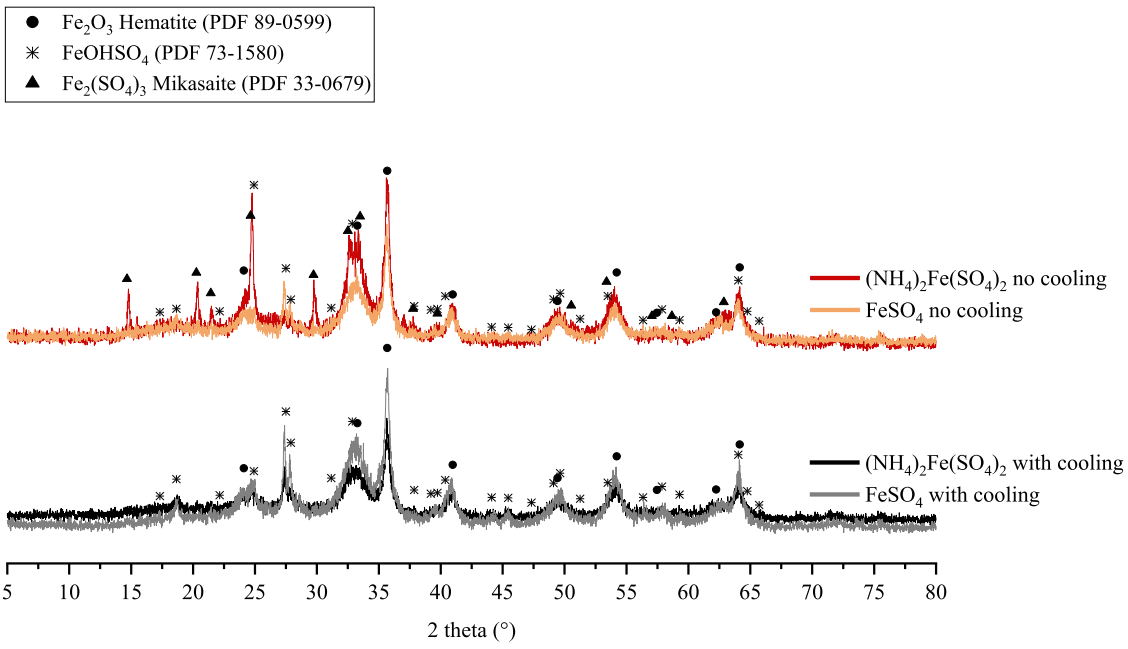

Fig. 3. XRD data of solids obtained with iron precursors with and without cooling system.

Table 3
XPS and EDX data of solids obtained with iron precursors with and without cooling system.

	Fe (at %)		O (at %)		S (at %)		N (at %)	Fe/O
	XPS (Fe2p)	EDX	XPS (O1s)	EDX *	XPS (S2p)	EDX	XPS (N1s)	XPS
$(NH_4)_2Fe(SO_4)_2$ with cooling	23.8	26	66.6	72	6.5	2	3.1	0.36
$(NH_4)_2Fe(SO_4)_2$ no cooling	23.6	26	67.6	72	7.1	5	1.7	0.35
$FeSO_4$ with cooling	26.4	28	66.8	69	6.8	3	/	0.40
$FeSO_4$ no cooling	26.7	19	67.4	76	5.9	6	/	0.40

* The at % of O obtained by EDX is likely overestimated due to the underlying adhesive tape used to fix the sample.

where heat is introduced, it is possible that the probability of collision between SO_4^{2-} and Fe^{3+} is heightened, consequently leading to the formation of a higher quantity of $FeOHSO_4$ phase. Since the rate of formation of $FeOHSO_4$ and FeOOH is less disparate when heat is applied, the likelihood of formation of one phase over the other becomes more similar. Consequently, this can result in a solid with a more homogeneous composition of phases, which is indeed what we observe, evidenced by the less pronounced difference in at % of S in the solid formed without the cooling system.

$$Fe^{2+} + NO_2^- + 2H^+ \rightarrow Fe^{3+} + NO^{\cdot} + H_2O \quad (4)$$

$$Fe^{3+} + 2H_2O \rightarrow FeOOH + 3H^+ \quad (5)$$

$$Fe^{3+} + SO_4^{2-} + H_2O \rightarrow FeOHSO_4 + H^+ \quad (6)$$

Furthermore, as already suggested before and also observed when the PD step is used, in the no cooling system, the $FeOHSO_4$ phase undergoes more decomposition due to the heating effect (Eq. (3)) [26]. As it partially decomposes into $Fe_2(SO_4)_3$, the at % of S increases, given that the S/Fe ratio in the $Fe_2(SO_4)_3$ phase (S/Fe =1.5) is higher than in $FeOHSO_4$ (S/Fe =1). This rise in the at % of S likely reflects the tendency of $FeOHSO_4$ to preferentially decompose into $Fe_2(SO_4)_3$ rather than into FeOOH under heating conditions. Notably, if the FeOOH phase (which subsequently decomposes into Fe_2O_3 through calcination) had preferentially developed instead of the $FeOHSO_4$ (Fe/O=0.2) and $Fe_2(SO_4)_3$ (Fe/O=0.17) phases, the Fe/O ratio would increase towards 0.67. However, observations of the Fe/O ratio in the solids developed without the cooling system reveal no change. This indicates that the Fe_2O_3 phase does not seem to develop better without the cooling system, at least at the surface of the solid (Table 3).

Regarding the morphology of the solids, unlike the observations made with the PD, it is evident that the no cooling system tends to result in solids with less specific surface area and pore volume (Table 4) [26].

Additionally, the SEM images for $FeSO_4$ precursor indicate that solids produced without the cooling system seem to have less texture on their surface. This may result from the agglomeration of the "flakes-like" particles typically observed when the cooling system is used (Fig. 4: (a) and (b)). However, it is difficult to conclude that this explains the decrease in specific surface area, as some particles appear to develop "sea-urchin like" crystals, which would normally increase the specific surface area of the solid (Fig. 4: (c)). In fact, it is noteworthy that these "sea-urchin like" crystals that are formed when the cooling system is omitted during the synthesis for $FeSO_4$ and $(NH_4)_2Fe(SO_4)_2$ precursors, are a characteristic structure not typically observed in conventional GP synthesis utilizing the cooling system (Fig. 4: (c), (d)). Nevertheless,

Table 4
Textural properties obtained by N2-physisorption with iron precursors with and without cooling system (isotherms Appendice B).

	Specific surface area (m^2/g)	Pore volume (cm^3/g)
$(NH_4)_2Fe(SO_4)_2$ with cooling	69	0.18
$(NH_4)_2Fe(SO_4)_2$ no cooling	32	0.13
$FeSO_4$ with cooling	95	0.33
$FeSO_4$ no cooling	23	0.11

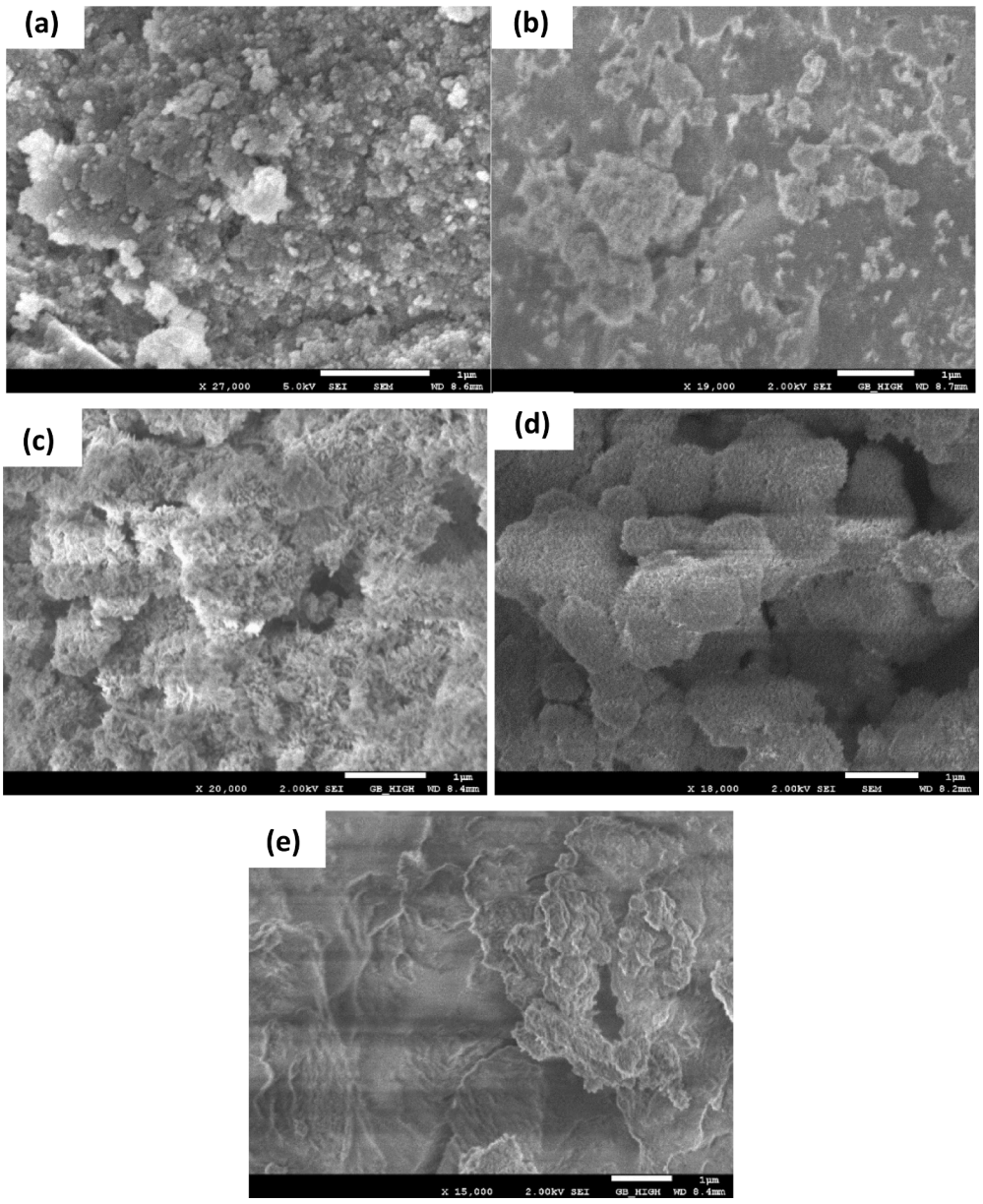

Fig. 4. SEM images of solids obtained with $FeSO_4$ (a) with cooling and (b), (c) without cooling system and obtained with $(NH_4)_2Fe(SO_4)_2$ (d), (e) without cooling system and.

these "sea-urchin like" crystals are not uniformly developed throughout the synthesized solids. In fact, certain particles resemble large, shapeless crystals that agglomerate together (Fig. 4: (b), (e)).

The literature explains that a PD step primarily involves a maturation process that facilitates crystal growth into the shape of a "sea-urchin like" structure, resulting in particles with a higher specific surface area in the case of solids derived from iron precursors [7,26]. In the absence of the cooling system, although the heat introduced during the synthesis seems to initiate the maturation of the crystals formed during the discharge, it does not afford sufficient time for the complete formation of these distinctive crystals. Consequently, direct application of heat during particles formation predominantly induces their agglomeration, thereby reducing the specific surface area of the catalyst.

With the information obtained from XRD, XPS, EDX, N_2-physisorption and SEM images, we can propose a mechanism of formation of the solids when iron precursors are exposed to the GP as illustrated in Fig. 5.

Concerning the catalytic activity of plasma-synthesized solids, a decline is observed when the cooling system is not used for both precursors (Fig. 6). This observation was expected as the absence of cooling system tends to result in the development of solids with a higher proportion of non-catalytically active phase ($Fe_2(SO_4)_3$) compared to the active phase (Fe_2O_3) and reduce their specific surface area and pore volume. In fact, compared to commercial Fe_2O_3 (iron(III) oxide, Alfa Aesar, 30-60 m^2/g), the catalytic activity of the developed solid is only comparable or better if the cooling system is used in the GP catalysts synthesis (Fig. 6). Consequently, in the case of solids derived from iron precursors, the no cooling system fails to impart beneficial characteristics able to compete those achieved with the cooling system and the PD step.

3.2.2. *Tin precursors*

Regarding the mass of the solid formed from tin precursors, it remains largely unchanged regardless of the presence or absence of the cooling system (Table 5). As explained before, contrary to what was observed when a PD step was applied, as the exposure time is identical in

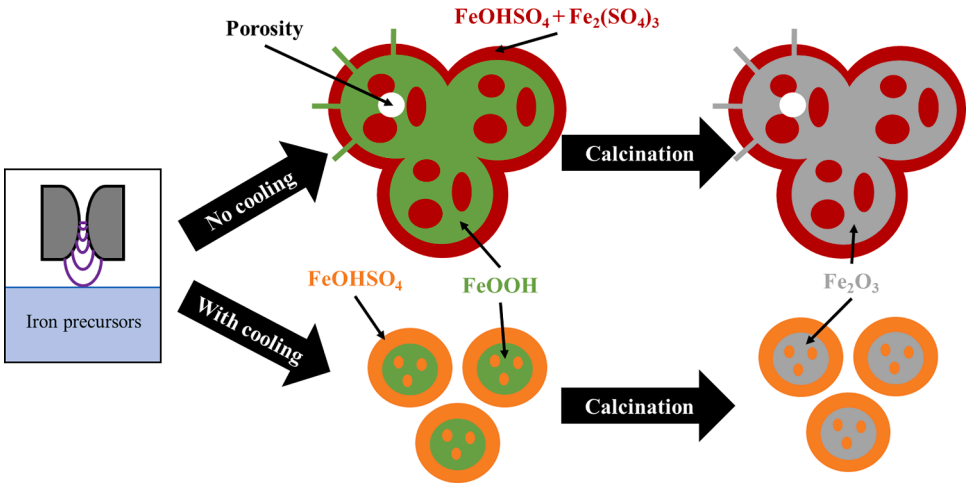

Fig. 5. Mechanism of formation of solids obtained with iron precursors with and without cooling system.

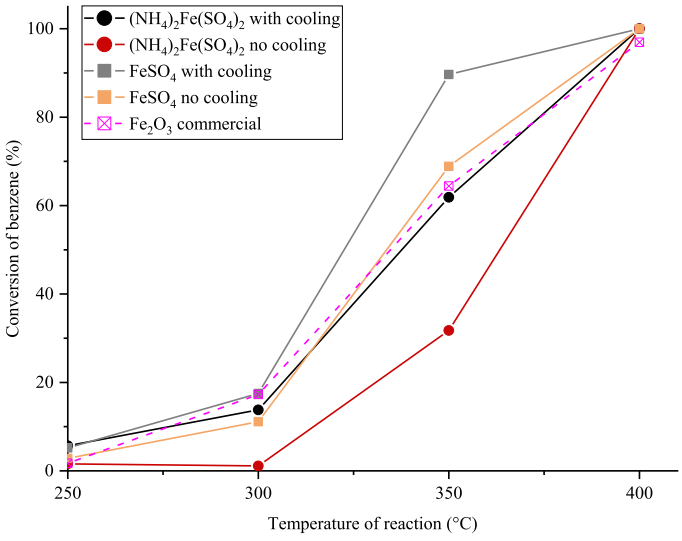

Fig. 6. Catalytic performances of solids formed from iron precursors with and without cooling system for the total oxidation of benzene (conversion of benzene as function of temperature reaction).

Table 5
Mass of solid produced with tin precursors by glidarc plasma with and without cooling system.

	Mass of solid produced (g)
$SnSO_4$ with cooling	0.686
$SnSO_4$ no cooling	0.622
$SnCl_2$ with cooling	0.674
$SnCl_2$ no cooling	0.704

both systems, the reactive species (HNO_2/NO_2^- [29]) do not have additional time to react with the precursor, resulting in an unchanged yield of precipitate solid.

The XRD diffractograms of the solids derived from tin precursors reveal that the phases developed with or without cooling system are the same. In both precursors, the phase developed is cassiterite (SnO_2), resulting from the dehydration of the $Sn(OH)_4$ formed in solution during the solid's drying steps (Fig. 7).

As observed for iron precursors, XPS and EDX data highlight that the at % of each element at the surface and in bulk consistently differs with or without cooling system, indicating the heterogeneous (bulk *vs* surface) composition of the precipitates (Table 6).

XPS data reveal the presence of sulfur (as SO_4^{2-}) for solids formed from $SnSO_4$ and Cl (as Cl^-)for $SnCl_2$ (as indicated by the positions of S2p and Cl1s, Appendice C), suggesting the likely formation of another phase that was not observed by XRD. Furthermore, the at % of S and Cl at the surface is consistently higher than in bulk, where they are almost negligible, implying that tin sulfate or tin chloride phases predominantly exist on the outer layer of the solids (Table 6).

XPS analysis also indicates that the at % of S or Cl is lower when the cooling system is absent, suggesting a diminished presence of sulfate or chloride phases at the surface (Table 6). Referring back to the proposed mechanism of solid formation from tin precursors outlined in [26], it is known that $SnCl_2$ and $SnSO_4$ undergo spontaneous hydrolysis to form hydroxychloride (SnOHCl) or hydroxysulfate ($Sn_3O(OH)_2SO_4$) intermediates. These intermediates are subsequently quickly oxidized by plasma species, resulting in the formation of tin hydroxide, $Sn(OH)_4$, which ultimately transforms into the more stable phase, SnO_2 (Eqs. (7–9)). Consequently, with the reduced presence of S or Cl at the surface of the solid in the absence of the cooling system, it can be inferred that the transformation of the intermediate phases occurs more efficiently under elevated temperatures. This inference is supported by the well-established tendency of Sn^{2+} ions to oxidize to Sn^{4+} at high temperatures, offering a plausible explanation for these observations [31, 32].

$$3SnSO_4 + 3H_2O \rightarrow Sn_3O(OH)_2SO_4 + 4H^+ + 2SO_4^{2-} \quad (7)$$

$$SnCl_2 + H_2O \rightarrow Sn(OH)Cl + HCl \quad (8)$$

$$Sn^{2+} + 2NO_2^- \rightarrow Sn(OH)_4 + 2NO^\circ + H_2O \quad (9)$$

However, looking at the Sn/O ratio of these solids, we cannot tell that the chloride and sulfate intermediates only undergo oxidation to form $Sn(OH)_4$, but they seem to also form another tin (hydr)oxide phase under heat (Table 6). If the $Sn_3O(OH)_2SO_4$ (Sn/O=0.43) or Sn(OH)Cl (Sn/O=1) intermediates were exclusively oxidized into SnO_2 (Sn/O=0.5), the Sn/O ratio of the resulting solid would be closer to 0.5. However, even with the cooling system, the value already exceeds 0.5 and is even higher without the cooling system (Table 6). Furthermore, as the at % of S or Cl indeed decreases, it means than another tin oxide phase with a higher Sn/O ratio is likely to form. It is conceivable that this phase corresponds to SnO (Sn/O=1) originating from $Sn_3O(OH)_2SO_4$ or Sn(OH)Cl, which were not oxidized but rather transformed into tin(II) oxide, namely an observation that was already made when a PD step was applied to a classical GP synthesis. Consequently, without the cooling system, it is plausible that a solid containing a mixture of SnO_2 and SnO

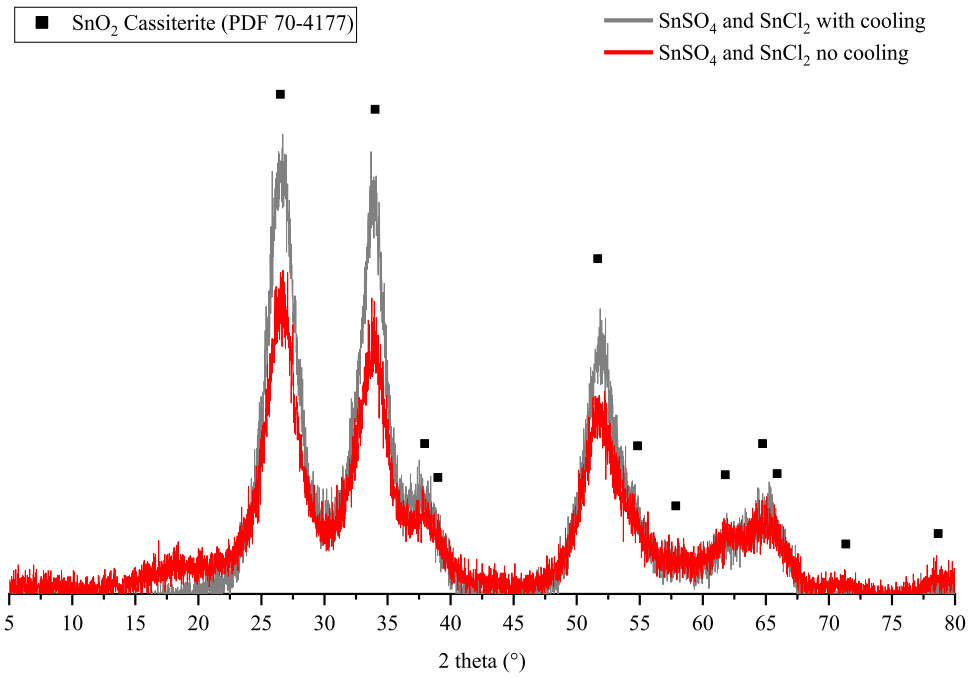

Fig. 7. XRD data of solids obtained with tin precursors with and without cooling system.

Table 6
XPS and EDX data of solids obtained with tin precursors with and without cooling system.

	Sn (at %)		O (at %)		S or Cl (at %)		Sn/O
	XPS (Sn3d)	EDX	XPS (O1s)	EDX *	XPS (S2p or Cl1s)	EDX	XPS
$SnSO_4$ with cooling	33.4	14	63.7	85	2.9	1	0.52
$SnSO_4$ no cooling	34.6	17	63.6	82	1.8	1	0.54
$SnCl_2$ with cooling	35.2	29	63.4	71	1.4	0	0.56
$SnCl_2$ no cooling	36.6	28	62.8	72	0.7	0	0.58

* The at % of O obtained by EDX is likely overestimated due to the underlying adhesive carbon tape used to fix the sample.

phases is generated, wherein less tin sulfate or tin chloride phases remain compared to the solid obtained when the cooling system is utilized in its preparation.

Regarding the texture of the solids, whether the cooling system is used or not, there is no substantial difference in the specific surface area or pore volume (Table 7). In contrast to observations made with the PD, applying heat to the system does not notably decrease the specific surface area. This is likely attributed to the fact that in the absence of the cooling system, the particles have less time to agglomerate compared to when a PD step is included in the synthesis protocol.

With the information obtained from XRD, XPS, EDX and N_2-physisorption, we propose a mechanism of formation of the solids when tin precursors are exposed to the GP as illustrated in Fig. 8.

Table 7
Textural properties obtained by N_2-physisorption with tin precursors with and without cooling system (isotherms Appendice D).

	Specific surface area (m^2/g)	Pore volume (cm^3/g)
$SnSO_4$ with cooling	162	0.13
$SnSO_4$ no cooling	142	0.14
$SnCl_2$ with cooling	146	0.11
$SnCl_2$ no cooling	164	0.10

Regarding the catalytic activity of solids derived from tin precursors, it is enhanced when the cooling system is not used (Fig. 9). These results align with the previously discussed characteristics. As the no cooling system facilitates the transformation of tin sulfate or chloride phases into more catalytically active phases (tin (IV and II) oxides) at the surface of the solid without altering the texture of the solids, it thereby enhances the catalytic activity of the obtained solids. Furthermore, compared to SnO_2 synthesized by classical precipitation with base (NH_3) addition precipitation, the tin-based catalysts synthesized by GP are already more catalytically active when the cooling system is used. However, their catalytic activity becomes even more competitive when the cooling system is not used [33].

3.3. Can the no cooling system replace the PD step in the GP catalysts synthesis?

We have previously shown that conducting a PD step either at 100 °C for 3 h or at 25 °C for 72 h irrespective of the precursor type, is an interesting process to increase the quantity of recovered solids and/or introduce intriguing new characteristics to the catalyst [26]. In fact, the PD effectively transforms the sulfate or chloride phases, which may have formed during the discharge, into metal oxides. Furthermore, it influences the textural properties of the solid, increases the amount of recovered solids and, in most cases, enhances its catalytic activity.

On the contrary, the no cooling system does not consistently yield beneficial characteristics to the solid generated by GP. When iron precursors are exposed to the GP without the cooling system, the resulting solids exhibit a higher proportion of $Fe_2(SO_4)_3$ and a reduced presence of the catalytically active phase (Fe_2O_3) compared to when the cooling system is utilized during the synthesis. Furthermore, the direct application of heat during particles formation predominantly promotes their agglomeration, leading to a decrease of specific surface area and pore volume of the catalyst. Consequently, this diminishes the catalytic activity of the formed solids. Conversely, in the case of tin precursors, solids developed without the cooling system exhibit a greater amount of catalytically active phase (tin (II and IV) oxides) and less tin sulfate or chloride phases remaining at the surface. Additionally, the specific

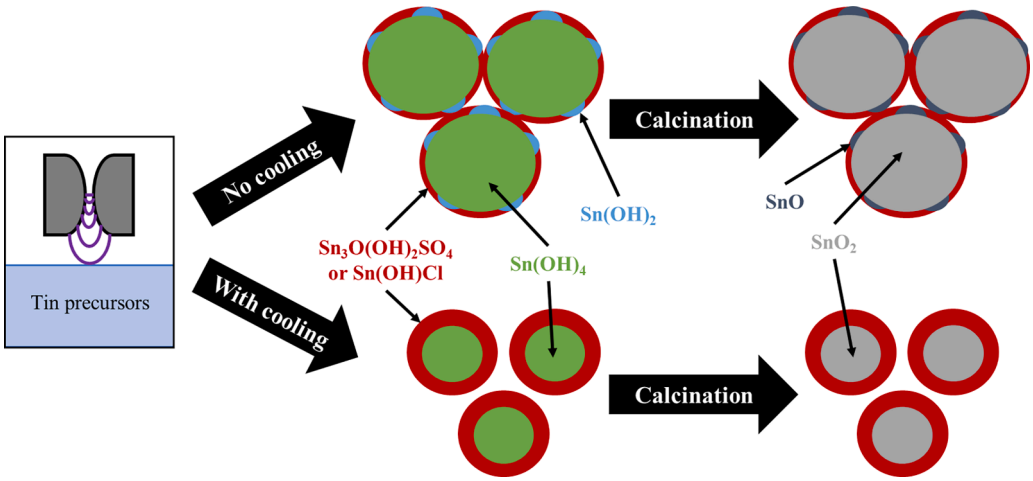

Fig. 8. Mechanism of formation of solids obtained with tin precursors with and without cooling system.

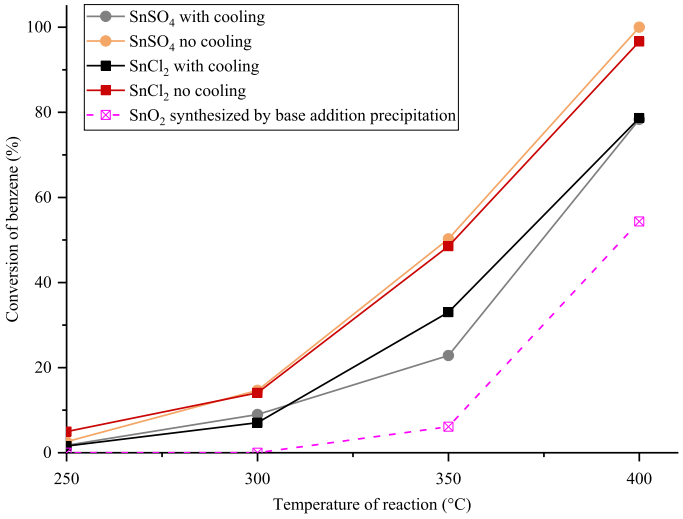

Fig. 9. Catalytic performances of solids formed from tin precursors with and without cooling system for the total oxidation of benzene (conversion of benzene as function of temperature reaction).

surface area remains relatively unaffected by the heat. Therefore, this results in a catalyst that is more active than when synthesized with the cooling system.

This finding is intriguing, particularly considering that conducting a PD at 100 °C for 3 h proved to be more beneficial for iron precursors than for tin precursors. It suggests that introducing heat during the PD step, also known as the maturation step, was advantageous for iron precursors, whereas this was not the case when heat was applied directly during the discharge, known as the nucleation step. Several factors may explain these differences. Firstly, the phases that emerge when iron precursors are subjected to discharge include $FeOHSO_4$ and FeOOH initially. However, as mentioned earlier, the formation of these phases is influenced by the introduction of heat, altering the rate at which one phase develops preferentially to another. Specifically, the elevated temperature probably increases the likelihood of collision between Fe^{3+} ions and SO_4^{2-}, thereby promoting the formation of the iron sulfate phase. Moreover, as observed when incorporating a PD step, the $FeOHSO_4$ phase produced during the discharge undergoes decomposition into $Fe_2(SO_4)_3$ and FeOOH, a process accelerated at elevated temperatures. Therefore, in the no cooling system, the addition of heat directly during the discharge already triggers the transformation of $FeOHSO_4$ that seems to also decompose into $Fe_2(SO_4)_3$ rather preferentially than FeOOH. Additionally, while elevated temperatures during synthesis appear to initiate the maturation of the solid into "sea-urchin-like" crystals, the direct application of heat during particle formation primarily induces their agglomeration, leading to a reduction in the specific surface area and pore volume of the catalyst. Consequently, for solids derived from iron precursors, it is unfavorable to introduce heat directly during the nucleation step instead of the maturation step. This is due to the way the ions present in the solution interact, the transformation of synthesized phases under heat, and the agglomeration effect induced by heat on particles.

On the other hand, employing a no cooling system for tin precursors yields intriguing characteristics that make catalysts even more active than when a PD step is incorporated in a conventional GP synthesis. Interestingly, as observed with the PD step, the introduction of heat into the system appears to improve either the oxidation of tin sulfate and tin chloride intermediates into SnO_2 or accelerate their decomposition into SnO. Consequently, the application of heat favours the formation of more catalytically active phases in the case of tin precursors. However, in the context of the PD step, increasing the synthesis duration and introducing heat during the PD step tends to cause particle agglomeration, thereby reducing their specific surface area. Conversely, with the no cooling system, we do not extend the synthesis time beyond the duration of discharge exposure, thereby avoiding the particle agglomeration observed in the PD step. Consequently, the specific surface area of the solid synthesized with or without a cooling system remains relatively unchanged. Thus, by employing the no cooling system with tin precursors, we develop the beneficial characteristics typically associated with a PD step without suffering its negative aspects. Ultimately, this approach enables the creation of more catalytically active solids by significantly reducing the synthesis time that would normally be required if a PD step were to be included.

4. Conclusion

In the aim of exploring the possibility of accelerating the maturation of GP-synthesized solids by directly applying heat during plasma exposure, we subjected various iron and tin precursors to plasma exposure without employing the cooling system and compared the resulting solids with those obtained through conventional synthesis involving a PD step at either 100 °C for 3 h or at 25 °C for 72 h.

Our findings showed that for iron precursors, the absence of cooling led to more less catalytically active phases ($FeOHSO_4$ and $Fe_2(SO_4)_3$) and fewer catalytically active phases (Fe_2O_3) compared to when the cooling system was employed during the synthesis. Moreover, the direct application of heat during particles formation induced their agglomeration, resulting in a reduction of specific surface area and pore volume,

consequently diminishing the catalytic activity of the formed solids.

In contrast, for tin precursors, solids developed without the cooling system had more catalytically active phases (tin (II and IV) oxides) and fewer less active tin sulfate or chloride phases on the surface. Additionally, the specific surface area was relatively unaffected by the heat. Therefore, this yielded a catalyst that was more active compared to that synthesized with the cooling system.

Therefore, we can conclude that, much like with the PD step, the results obtained vary from one precursor to another, while following a discernible pattern for precursor salts of the same metal. For certain precursors, the absence of a cooling system cannot replicate the interesting characteristics developed with the PD step, while for others, it appears to introduce even more intriguing features. When favourable, the no cooling system becomes notably interesting, as it can potentially replace the PD step. In fact, in the no cooling approach, no additional heat is introduced, as we allow the solution to be heated by the energy naturally provided by the plasma discharge. Consequently, this drastically reduces the energy cost of the synthesis. Additionally, we can significantly decrease the synthesis time, thereby reducing both the energy and economic impacts of the synthesis. This system could, therefore, represent an interesting approach to improving the overall GP catalyst synthesis process, by reducing its environmental and economic footprint.

CRediT authorship contribution statement

Fanny Hanon: Supervision. **Eric Michel Gaigneaux:** Writing – original draft.

Declaration of competing interest

The authors declare the following financial interests/personal relationships which may be considered as potential competing interests:

Hanon fanny reports financial support was provided by Fund for Scientific Research. If there are other authors, they declare that they have no known competing financial interests or personal relationships that could have appeared to influence the work reported in this paper

Data availability

Data will be made available on request.

Acknowledgments

Fanny Hanon acknowledges the FNRS for the FRIA scholarship no.40004581.

The authors gratefully acknowledge François Devred for the technical and logistical support and Michel Devillers and Sophie Hermans for the chemistry private lessons and advices.

Supplementary materials

Supplementary material associated with this article can be found, in the online version, at doi:10.1016/j.apmt.2024.102408.

References

[1] J.M. Thomas, W.J. Thomas, Principles And Practice Of Heterogeneous Catalysis, VCH, Weinheim, 1997.
[2] D. Kolb, Catalysis, J. Chem. Educ. 56 (1979) 743–747.
[3] J. Védrine, Heterogeneous catalysis on metal oxides, Catalysts 7 (2017) 341.
[4] L. Lerner, 7 things you may not know about catalysis, Argonne Natl. Lab. (2011). https://www.anl.gov/article/7-things-you-may-not-know-about-catalysis.
[5] J.W. Niemantsverdriet, Spectroscopy in Catalysis : An Introduction, 2nd ed., Wiley-VCH, Weinheim, 2000.
[6] J.F. Lepage, Catalyse De Contact : Conception, Préparation Et Mise En Oeuvre Des Catalyseurs Industriels, Technip, Paris, 1978.
[7] A. Tiya-Djowe, S. Laminsi, G.L. Noupeyi, E.M. Gaigneaux, Non-thermal plasma synthesis of sea-urchin like α-FeOOH for the catalytic oxidation of Orange II in aqueous solution, Appl. Catal. B Environ. (2015) 99–106, 176–177.
[8] A. Czernichowski, Gliding arc: Applications to engineering and environment control, Pure Appl. Chem. 66 (1994).
[9] H. Lesueur, A. Czernichowsky, J. Chapelle, Dispositif de génération de plasma basse température par formation de décharges électriques glissantes, 2639172, n.d.
[10] M.R. Ghezzar, F. Abdelmalek, M. Belhadj, N. Benderdouche, A. Addou, Gliding arc plasma assisted photocatalytic degradation of anthraquinonic acid green 25 in solution with TiO2, Appl. Catal. B Environ. 72 (2007) 304–313.
[11] E.B. Tsagou-Sobze, D. Moussa, A. Doubla, E. Hnatiuc, J.L. Brisset, Gliding discharge-induced oxidation of a toxic alkaloid, J. Hazard. Mater. 152 (2008) 446–449.
[12] A. Czernichowski, H. Nassar, A. Ranaivosoloarimanana, A.A. Fridman, M. Simek, K. Musiol, E. Pawelec, L. Dittrichova, Spectral and electrical diagnostics of gliding arc, Acta Phys. Pol. A 89 (1996) 595–603.
[13] A. Doubla, L. Boubabello, M. Fotso, J. Brisset, Plasmachemical decolourisation of Bromothymol Blue by gliding electric discharge at atmospheric pressure, Dyes Pigments 77 (2008) 118–124.
[14] A. El-Zein, M. Talaat, G. El-Aragi, A. El-Amawy, Electrical characteristics of nonthermal gliding arc discharge reactor in argon and nitrogen gases, IEEE Trans. Plasma Sci. 44 (2016) 1155–1159.
[15] J.L. Brisset, D. Moussa, A. Doubla, E. Hnatiuc, B. Hnatiuc, G. Kamgang Youbi, J. M. Herry, M. Naïtali, M.N. Bellon-Fontaine, Chemical reactivity of discharges and temporal post-discharges in plasma treatment of aqueous media: examples of gliding discharge treated solutions, Ind. Eng. Chem. Res. 47 (2008) 5761–5781.
[16] F.W.B. Tatchemo, S. Nzali, G. Kamgang Youbi, A. Tiya Djowe, D.K. Saa, E. Acayanka, S. Laminsi, E.M. Gaigneaux, Gliding arc plasma synthesis of mno2 nanorods for the plasma-catalytic bleaching of azoïc amaranth red dye, Top. Catal. 60 (2017) 962–972.
[17] A. Tiya-Djowe, E. Acayanka, A.P. Mbouopda, W. Boyom-Tatchemo, S. Laminsi, E. M. Gaigneaux, Producing oxide catalysts by exploiting the chemistry of gliding arc atmospheric plasma in humid air, Catal. Today 334 (2019) 104–112.
[18] J.L. Brisset, J. Pawlat, Chemical effects of air plasma species on aqueous solutes in direct and delayed exposure modes: discharge, post-discharge and plasma activated water, Plasma Chem. Plasma Process 36 (2016) 355–381.
[19] B. Benstaali, P. Boubert, B.G. Cheron, A. Addou, J.L. Brisset, Density and rotational temperature measurements of the OH° and NO° radicals produced by a gliding arc in humid air, Plasma Chem. Plasma Process. 22 (2002) 553–571.
[20] D. Moussa, H. Vitrac, B.G. Chéron, E. Hnatiuc, A. Addou, J.L. Brisset, Acidity control of the oxidation reactions induced by non-thermal plasma treatment of aqueous effluents in pollutant abatment processes, Eur. Phys. J. Appl. Phys. 29 (2005) 308–312.
[21] E. Acayanka, D.S. kuete, G.Y. Kamgang, S. Nzali, S. Laminsi, P.T. Ndifon, Synthesis, characterization and photocatalytic application of TiO2/SnO2 nanocomposite obtained under non-thermal plasma condition at atmospheric pressure, Plasma Chem. Plasma Process. 36 (2016) 799–811.
[22] A.P. Mbouopda, E. Acayanka, F.W. Boyom-Tatchemo, G.Y. Kamgang, A.M. Nzeufa, S. Laminsi, D. Richard, New-route synthesis of N-doped TiO2 via exposing the TiCl3 precursor to non-thermal quenched plasma at various times, Mater. Chem. Phys. 206 (2018) 224–231.
[23] A. Tiya-Djowe, M.A. Dourges, H. Deleuze, Tuning the "O" vacancies density in SnO2 nanocrystals during and after humid air plasma synthesis: implications on the photocatalytic performances under UV light, J. Mater. Sci. 55 (2020) 4792–4807.
[24] F.W. Boyom-Tatchemo, F. Devred, G. Ndiffo-Yemeli, S. Laminsi, E.M. Gaigneaux, Plasma-induced redox reactions synthesis of nanosized α-, γ- and δ-MnO2 catalysts for dye degradation, Appl. Catal. B Environ. 260 (2020) 118159.
[25] F.W. Boyom-Tatchemo, F. Devred, S. Laminsi, E.M. Gaigneaux, Temporal post-discharge reactions effect on the oxidative catalytic properties of plasma-synthesized α-MnO2 nanorods, Appl. Catal. Gen. 616 (2021) 118109.
[26] F. Hanon, E.M. Gaigneaux, Post-discharge: An interesting step to improve heterogeneous catalysts synthesized by glidarc plasma? Chem. Eng. J. 489 (2024) 151088.
[27] A. Tiya Djowe, Adsorbants et catalyseurs à base d'argile préparés par voie plasmachimique pour la dépollution des eaux résiduaires industrielles, Thèse, Université catholique de Louvain, Université de Yaoundé I, 2014.
[28] The International Centre for Diffraction Data, ICDD (2020). http://www.icdd.com/.
[29] F. Hanon, S. Hermans, E.M. Gaigneaux, What are the species involved in the gliding arc plasma synthesis of heterogeneous catalysts? Catal. Today 430 (2024) 114550.
[30] P.K. Gallagher, D.W. Johnson, F. Schrey, Thermal Decomposition of Iron(II) Sulfates, J. Am. Ceram. Soc. 53 (1970) 666–670.
[31] J. Wang, H. Li, S. Meng, X. Ye, X. Fu, S. Chen, Controlled synthesis of Sn-based oxides via a hydrothermal method and their visible light photocatalytic performances, RSC Adv. 7 (2017) 27024–27032.
[32] E. Ovodok, M. Ivanovskaya, D. Kotsikau, I. Azarko, V. Kormosh, I. Alyaksev, Effect of structure and surface state ofnanocrystalline tin dioxide on its gas sensing properties, Phys. Chem. Appl. Nanostructures (2013) 625–628. , world scientific, Minsk, Belarus.
[33] A. Ghaderi, S. Abbasi, F. Farahbod, Synthesis of SnO2 and ZnO nanoparticles and SnO2-ZnO hybrid for the photocatalytic oxidation of methyl orange, Irian J. Chem. Eng. 12 (2015).